Fully Automatic Segmentation of the Brain in MRI

M. Stella Atkins* and Blair T. Mackiewich, *Member, IEEE*

***Abstract*— A robust fully automatic method for segmenting the brain from head magnetic resonance (MR) images has been developed, which works even in the presence of radio frequency (RF) inhomogeneities. It has been successful in segmenting the brain in every slice from head images acquired from several different MRI scanners, using different-resolution images and different echo sequences.**

The method uses an integrated approach which employs image processing techniques based on anisotropic filters and "snakes" contouring techniques, and *a priori* knowledge, which is used to remove the eyes, which are tricky to remove based on image intensity alone. It is a multistage process, involving first removal of the background noise leaving a head mask, then finding a rough outline of the brain, then refinement of the rough brain outline to a final mask.

The paper describes the main features of the method, and gives results for some brain studies.

***Index Terms*— Anisotropic filter, MRI brain, segmentation, snakes.**

I. Introduction

MAGNETIC resonance imaging (MRI) provides detailed images of living tissues, and is used for both brain and body human studies. Data obtained from MR images is used for detecting tissue deformities such as cancers and injuries; MR is also used extensively in studies of brain pathology, where regions of interest (ROI's) are often examined in detail, for example in multiple sclerosis (MS) studies [36], [35]. In order to perform good quantitative studies, ROI's within the brain must be well defined. In traditional methods, a skilled operator manually outlines the ROI's using a mouse or cursor. More recently, computer-assisted methods have been used for specific tasks such as extraction of MS lesions from MRI brain scans [23], [47], or extraction of the cerebral ventricles in schizophrenia studies [15]. Many of these computer-assisted tasks require segmentation of the whole brain from the head, either because the whole brain *is* the ROI such as in Alzhiemer's studies [18] or because automatic ROI extraction using statistical methods is made easier if the skull and scalp have been removed [23].

We describe our automatic method for segmenting the brain from the head in MR images. The key to any automatic method is that it must be robust, so that it produces reliable results on every image acquired from any MR scanner using different relaxation times, slice thicknesses and fields of view. Our method is so robust, that it successfully was able to segment the brain in every slice of 40 head images from five different MRI scanners (all 1.5-T; four from GE, one from Siemens), using several different spin-echo images with different echo times, and with two T1-weighted gradient pulse sequences. Our method works in the presence of typical radio frequency (RF) inhomogeneity and it addresses the partial volume effect in a consistent reasonable manner. The method is partly two-dimensional (2-D)-based and partly three-dimensional (3-D)-based, and it works best on routine axially displayed multispectral dual-echo proton density (PD) and T2 (spin-spin relaxation time) sequences. It also works well on axial and coronal 3-D T1-weighted SPGR (Spoiled Gradient) sequences. However, it does *not* work fully automatically on sagitally displayed 3-D T1-weighted images where accurate localization of cortical convolutions is required, as parameter tuning is necessary to include the thin dark brain areas and keep the cerebellum attached to the rest of the brain, while simultaneously separating the brain from the back of the neck tissue and the cheeks. For such sagitally displayed images, other techniques such as those described in [1], [13], [19], and [24] are available. The computer processing time for each study for all the stages was less than five minutes on a SUN SPARC workstation—even for the 120 slice 3-D studies.

For segmentation of the brain, hybrid methods incorporating both image-processing and model-based techniques are useful [1], [4], [24]. Our hybrid method is typical in that it involves some image processing steps first: *viz.* a thresholding step followed by a morphological erosion to remove small connections between the brain and surrounding tissue. A model-based approach is then used to eliminate the eyes and other nonbrain features, followed by more image processing consisting of a morphological dilation to recover some of the eliminated tissue and a final refinement of the brain contour (in our case, using Terzopoulos and Kass's "snakes" active contour algorithm [25]).

Our method is unique in that it is possible to select the image processing parameters automatically; in particular, the thresholding parameter is found by applying an anisotropic diffusion filter to the image and locating a threshold based on the characteristics of the resulting voxel intensity histogram.

A. Previous Work

The survey by Clarke *et al.* of segmentation methods for MR images [11] describes many useful image processing techniques and discusses the important question of validation. The various image processing techniques used for segmenting

Manuscript received August 22, 1996; revised February 6, 1998. This work was supported in part by the Natural Sciences and Engineering Research Council of Canada and the Multiple Sclerosis Society of Canada. The Associate Editor responsible for coordinating the review of this paper and recommending its publication was L. P. Clarke. *Asterisk indicates corresponding author.*

*M. S. Atkins is with the School of Computing Science, Simon Fraser University, Burnaby, B.C., V5A 1S6 Canada (e-mail: stella@cs.sfu.ca).

B. T. Machiewich is with the School of Computing Science, Simon Fraser University, Burnaby, B.C., V5A 1S6 Canada.

Publisher Item Identifier S 0278-0062(98)03304-7.

the brain can be divided into several groups: those required to perform a crude threshold-based extraction of the brain, followed by refinement of brain contours; statistical methods for brain segmentation, and region growing methods.

1) Brain Extraction Using Automatic Thresholding: Suzuki and Toriwaki use iterative thresholding to distinguish brain tissues from others in axial MR slices [43]. Starting at set values, thresholds for the head and the brain are then iteratively adjusted based on the geometry of resulting masks (i.e., the head mask includes the brain mask). This method is ineffective in the presence of RF inhomogeneity and in slices where the brain is not one homogeneous region closely surrounded by the skull.

Li *et al.* use knowledge-based thresholding in multimodal MRI data to classify voxels into multiple intensity categories [27]. In each axial slice, they compute the centroid of voxels categorized as brain. Next, four points defining a quadrangle are found at the edge of the brain by tracing left, right, up, and down from the centroid to a transition in tissue categories. All voxels outside the quadrangle that are not categorized as brain tissue are then masked to define the intracranial contour. Obviously, this method works only in slices where the brain constitutes one fairly homogeneous region.

Brummer *et al.* use histogram analysis and morphology to generate a 3-D brain mask [8]. Using a model of background noise, they first automatically generate a mask of the head and perform intensity correction on the masked volume. Next they create an initial brain mask using an automatic threshold based on a presupposed brain voxel intensity distribution. They then eliminate regions in the brain mask that are too close to the edge of the head. Finally, they use novel morphological operations to clean up the resulting mask. This method misses brain tissue in extreme slices and includes nonbrain tissues in others. In some cases it produces errors near the eyes. The method relies on *a priori* intensity correction to deal with RF inhomogeneity, so cannot be used retroactively.

Aboutanos and Dawant [1] use histogram analysis to determine the threshold selection in 3-D T1-weighted magnetization-prepared rapid gradient echo (MP-RAGE) data sets where the grey matter appears darker than the white; they choose as a lower threshold the peak intensity of the grey matter, and an upper threshold in the vicinity of the upper boundary of the white matter, where the brain lobe starts to flatten. These parameters can be automatically located, but the resulting brain segmentation may underestimate the grey matter and may still allow attachment of the dura to the brain in certain images. Furthermore, their method for evaluating threshold values is unique to the MP-RAGE acquisition sequence. However, we have incorporated their thresholds for 3-D MP-RAGE volumes in our algorithm with some success, although our results have yet to be validated.

2) Refinement of Brain Contour: Aboutanos and Dawant [1] describe a geometric deformable model used to refine an initial brain mask. Their deformable model uses the pixel intensity along lines which are placed approximately perpendicular to the initial contour. A five-term cost matrix is associated with transforming the image to hug the contours; in addition, a sixth term is required to repel the optimum curve from image locations such as eye and skin locations in T1-weighted images. The authors have found values for these parameters which perform well on sagitally displayed brain contours of 3-D T1-weighted MP-RAGE volumes on many volunteers, although the method requires a very good initial contour and excess fat can affect results. Two iterations are applied, and the blurred image is used to reduce the effect of noise. This method looks very promising, but no results are presented for PD and T2-weighted images.

Chakraborty *et al.* combine statistical segmentation and boundary detection to isolate features in MR images [9]. They first segment the images using a method similar to the iterated conditional modes (ICM) algorithm [22]. They then use a parametrically deformable shape model algorithm to find the boundary of interesting features in the segmented image [41]. The shape model algorithm modifies the shape of a predefined closed contour to match the shape of a ROI. This method requires user interaction to seed the segmentation and provide an initial shape contour. Further, the segmentation may fail due to RF inhomogeneity.

Snell *et al.* use an active surface template to find the intracranial boundary in MRI volumes of the head [40]. The method is based on the active contour model algorithm, "Snakes" [25]. Given an initial estimate of an object boundary, "Snakes" approaches the actual boundary by solving an energy minimization problem. In Snell's method, the user identifies points in the MR image that correspond to points on a "standard" active surface template of the brain. Based on these points, the template is registered to the image. The "Snakes" algorithm is then used to attract the surface template to the intracranial boundary. Snell's method appears to work better than all the other methods discussed herein. However, Snell used high-resolution isotropic 3-D MRI data to test his algorithm. Such MRI scans are generally not performed clinically. Still, the method requires user interaction and may fail for images that do not contain the entire brain.

Snakes have been used successfully to extract the contours from cardiac MRI studies [38] by propogating the snake from one image to another, with an intermediate processing step to provide a better starting contour, which prevents the snake contour from becoming trapped in incorrect local minima. This study highlights the need to provide a good initial contour for subsequent snake contour refinement; a lesson which we learnt early in our research too.

Davatzikos and Prince propose the use of a new active contour algorithm for ribbons (ACAR), which is specifically designed for mapping the human cortex [14]. Their initial results are promising, but the examples given are not visually superior to our results using snakes, although their method may prove better than snakes at tracking into cortical convolutions.

Lobregt and Viergever [30] propose a different dynamic contour model based on deformation of a set of vertices connected by edges. The deformation is caused by acceleration forces acting on the vertices; the forces are internal (derived from the shape of the contour model) and external (derived from some image feature energy distribution). At each deformation step, the new position of each vertex is calculated; after a number of steps, a stable end situation is reached when both

velocity and acceleration are zero for each vertex. Preliminary results applying this technique show its promise in tracking edges in 2-D medical images, although it is very sensitive to the initial contours provided.

Thedens *et al.* [44] proposed another method to search for borders in MR images, based on graph searching for minimum cost edge detection applied to a temporal or spatial sequence of images. This method has been shown to work on cardiac MR images, but it cannot be used on a single image volume—a sequence of several images is required—and it is computationally very expensive.

Lundervold and Storvik proposed a segmentation method for brain parenchyma in the central slices of multispectral MR images [31] which uses a model-based segmentation method and also uses a new Bayesian dynamic contour (BDC) model to detect the boundaries. The advantage of this approach over the snakes active contour is that the energy functions used to find the boundary can be more generally based on information about the whole region, rather than just the local boundary characteristics. The results are promising for the central slices of multispectral images presented, but have yet to be developed for isolating the whole brain, or for working with just a single echo sequence.

Li *et al.* [28] have developed a knowledge-based segmentation technique called "edgementation" which allows identification of the brain contours in computed tomography (CT) images, upon which they use a boundary refinement algorithm to improve the brain boundary. This algorithm maximizes an optimization function of the gradient, the orientation change of the gradient and the local curvature. The results are given for fairly smooth contours of the brain in axial CT slices, and it is not known if the algorithm is able to track the cortex in MR images.

Automatic skull boundary detection for the purposes of automatic registration of CT and MR head images has been developed by Van den Elsen *et al.* [16], based on the fact that the MRI signal forms a trough at the skull. In certain MRI slices the skull boundary is close to the brain boundary, but this cannot be used in general to segment the brain.

3) Statistical Methods for Brain Segmentation: The review by Bezdek *et al.* of statistical techniques [24] describes many supervised and unsupervised statistical methods for MR segmentation in general, and discusses their possibilities and limitations.

Kapur *et al.* [24] combine Well's statistical classification of MR images [46] with image processing methods, to segment the brain in 3-D gradient-echo MR images. They use a single-channel, nonparametric, multiclass implementation of Well's classifier based on tissue type training points to classify brain tissues. The resulting segmented brain requires further morphological processing to remove connected nonbrain components. The established brain contours are refined using a snake-based algorithm. The combination of statistical classification of brain tissue, followed by morphological operators, does well in segmenting brain from orbits etc. in a semiautomated fashion. Furthermore, Well's statistical classification method also reduces the effect of RF inhomogeneity. However, Kapur's method requires some interaction to provide tissue training pixels and in 10% of volumes studied interaction is needed to remove nonconnected brain tissue. The method is also computationally expensive, and has only been used on 3-D T1 gradient-echo data with slice thickness of 1.5 mm. It is not clear whether the technique will provide satisfactory segmentation of PD-T2 images with slice thickness of 5 mm.

Cline *et al.* segment the brain from MR images of the head using statistical classification [12]. To segment the brain, samples of brain voxels and nonbrain voxels are interactively identified. Bivariate normal distributions, corresponding to the different tissue types in the PD-weighted and T2-weighted MR images, are fitted to the sampled intensities. All the image voxels are then classified according to where their intensities lie in the distributions. Finally, the results are smoothed to remove discontinuities in classified regions. This method requires user interaction, fails in the presence of RF inhomogeneity, and falsely classifies nonbrain regions, such as the eyes, as brain.

Lachmann and Barillot isolate brain tissues in MRI slices using several texture analysis methods [26]. They use texture information to create an initial voxel classification. Cluster analysis and Bayesian relaxation is then used to refine the classification. Lachmann and Barillot do not show results for slices containing the eyes or the mouth. Bayesian relaxation-based techniques confuse these features with brain tissue [23].

Stringham *et al.* use a statistical relaxation method that incorporates gradient magnitude as well as voxel intensity for brain segmentation [42]. This segmentation algorithm is robust in the presence of RF inhomogeneity, but confuses tissues, such as the eyes, with brain tissue. Further, user interaction is required to seed the relaxation process.

Vinkin *et al.* use probabilistic hyperstacks for 2-D image segmentation [45]. A hierarchical stack of decreasing-resolution images is produced by progressively low pass filtering the original. Pixels in high-reslution images (children) are probabilistically linked to voxels in low-reslution images (parents) according to an objective criterion. Features of interest are identified in a low-reslution image and propagated to all siblings, weighted by the linked probabilities. Thus, a statistical segmentation is produced. Identifying the features of interest and thresholding the final segmentation must be performed manually in this method.

4) Region Growing and Boundary Detection: Pannizzo *et al.* detect the intracranial boundary in axial MRI slices by tracing a horizontal line outwards from the center of the image [34]. The point, in each direction, at which the voxel intensity under the line drops below a reference threshold is considered to be a point in the intracranial boundary. A running average of voxel intensities under the line is then computed. The intracranial boundary points are relocated to the first voxels with an intensity too far below the average. The running-average procedure is repeated for rows in the image. The entire process is then repeated for all columns. The result is a sequence of points defining the intracranial contour. This method can only detect the contour in slices where the brain is one homogeneous region and may not cope well with RF inhomogeneity.

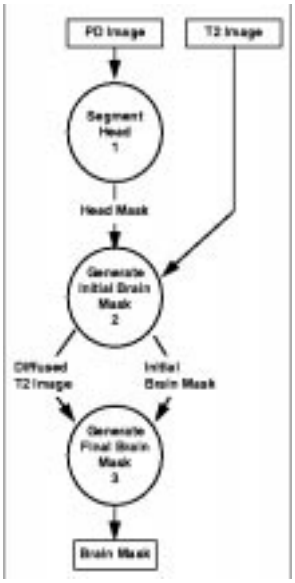

Fig. 1. A simplified data flow diagram representing automatic intracranial boundary detection.

Lim and Pfefferbaum [29] and Attwood *et al.* [6] trace lines radially outward from the approximate center of the head in an approach similar to that proposed by Pannizzo *et al.* Attwood *et al* impose a smoothness criterion on the resulting contour to refine the location of the intracranial boundary. Zijdenbos *et al.* fit a surface to the voxel intensities under the contour produced by [29] in order to produce a local threshold [47]. The radial line tracing algorithm is then repeated using the threshold to choose the voxels at the intracranial boundary. Zijdenbos' method is more robust than the others in the presence of RF inhomogeneity and partial volume effects. However, none of these methods works for slices where the brain is separated into two or more disjoint regions.

The remainder of the paper describes the method we use, and gives some results. We then provide a summary with an outline of future work.

II. Method

A. Overview

We use a three-stage method to segment images as shown in Fig. 1. First we remove the background noise, then we generate an initial mask for the region(s) of interest, then we refine the mask for the final segmentation. Each stage (bubble) in the diagram has been implemented using the WiT visual programming environment [3], which aids prototype development and enables experimentation [5].

The first stage, *Segment Head*, uses intensity histogram analysis to remove background noise and provide a head mask defining the head.

The second stage, *Generate Initial Brain Mask*, produces a mask that approximately identifies the intracranial boundary. A head image is filtered using a nonlinear anisotropic diffusion filter, to identify regions corresponding to the brain. The T2-weighted image is used if it is available, else the PD-weighted or T1-weighted image may be used. The nonlinear anisotropic diffusion effectively counters RF inhomogeneity by smoothing the brain regions and by reducing the intensity of the narrow nonbrain regions such as the scalp.

With the initial brain mask as a seed, the third step, *Generate Final Brain Mask*, locates the intracranial boundary using an active contour model algorithm. The active contour model algorithm consistently tracks the edge of the brain, even in the presence of partial volume effects.

Stages 1 and 3 require no *a priori* information about the organ to be segmented. Knowledge about the organ of interest is used only in the second stage, in which the initial brain mask is generated. We use two expert pieces of information. One allows us to eliminate nonbrain tissues such as the eyes, using morphology, by exploiting the simple fact that the brain centroid must be near the centroid of the slice. The other item of knowledge is that the brain tissues appear in MR images with relatively high intensity and when the T2 (or PD) image is filtered with a special anisotropic diffusion filter, most of the nonbrain tissues can be darkened, and hence the brain tissues can be segmented using a simple threshold. The methodology is described in more detail below, and in full detail in [32]. Although seemingly complex, the method has proven so robust that it works even in the presence of RF inhomogeneity, which would not be the case if a simple threshold technique were used to identify brain tissue from nonbrain tissue.

B. Segment Head

The head mask is generated using the method suggested by Brummer *et al.* to determine the "best" threshold level for removing background noise in PD-weighted MR images [8]. The method is based on the fact that MR scanners produce normally distributed white noise [17]. Henkelman [21] showed that background noise in reconstructed MR volumes has a Rayleigh distribution

$$p_{\text{noise}}(f) = \frac{f}{\sigma^2} \exp\left(-\frac{f^2}{2\sigma^2}\right) \tag{1}$$

where f is the noise intensity and σ is the standard deviation of the white noise. Fig. 2 shows that this distribution is easily visible in the low intensity range of the uncorrected MRI histogram.

The subtraction of the best-fit Rayleigh curve, $r(f)$, from the volume histogram, $h(f)$, produces a bimodal distribution

$$g(f) = h(f) - r(f). \tag{2}$$

A minimum error threshold τ can be determined from $g(f)$ by minimizing an error term ε_τ

$$\varepsilon_\tau = \sum_{f=0}^{\tau-1} g(f) + \sum_{f=\tau}^{\infty} r(f). \tag{3}$$

Fig. 3 shows the results of automatically thresholding an MR volume using this method. The binary image in Fig. 3(b) produced by thresholding the volume at τ, contains speckle outside the head region and has misclassified regions within the head. This "noise" is easily removed using standard morphological operations—we used a 5×5 kernel, detailed in [32].

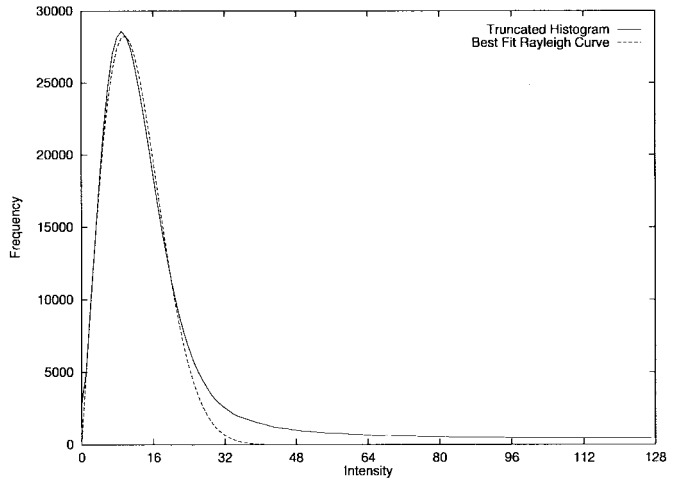

Fig. 2. A truncated histogram of a PD-weighted MR volume. The background noise at the low end of the histogram is characterized by a Rayleigh distribution.

(a) (b) (c)

Fig. 3. A head mask produced using automatic thresholding and morphology. (a) Original image. (b) Initial head mask. (c) Final head mask after morphology.

C. Generate Initial Brain Mask

This is a three step process which first uses 2-D nonlinear anisotropic diffusion to smooth the brain and attenuate narrow nonbrain regions such as the scalp in each MRI slice. Next, it automatically thresholds the diffused MR volume to produce a binary mask. Finally, misclassified, nonbrain regions are removed from the binary mask using morphology and spatial information provided by the head mask.

1) Nonlinear Anisotropic Diffusion: These are iterative, "tunable" filters introduced by Perona and Malik [37]. Gerig *et al.* used such filters to enhance MR images [20]. Sapiro and Tannenbaum used a similar technique to perform edge preserving smoothing of MR images [39]. Others have shown that diffusion filters can be used to enhance and detect object edges within images [33], [37], [2].

Perona and Malik formulate the anisotropic diffusion filter as diffusion process that encourages intraregion smoothing while inhibiting interregion smoothing

$$\frac{\partial}{\partial t} I(\bar{x},t) = \nabla \cdot (c(\bar{x},t)\nabla I(\bar{x},t)). \tag{4}$$

In our case, $I(\bar{x},t)$ is the MR image. $\bar{x}$ refers to the image axes (i.e., x,y) and t refers to the iteration step. $c(\bar{x},t)$ is called the *diffusion function* and is a monotonically decreasing function of the image gradient magnitude. It allows for locally adaptive diffusion strengths: edges are selectively smoothed or enhanced based on the evaluation of the diffusion function. We use the following diffusion function in our algorithm [37]:

$$c(\bar{x},t) = \exp\left(-\left(\frac{|\nabla I(\bar{x},t)|}{\sqrt{2}\,\mathcal{K}}\right)^2\right). \tag{5}$$

$\mathcal{K}$ is referred to as the *diffusion constant* or the *flow constant*, and the behavior of the filter depends on $\mathcal{K}$. For all our images we used the same value of $\mathcal{K} = 128$ with 25 iterations and a time step value of just under 0.2, as these values consistently produced a sufficiently blurred image for thresholding. Although the filtering is fairly sensitive to these three parameters, we found that for *all* the PD-, T2-, and T1-weighted data sets axially or coronally displayed, the above setting for the parameters allowed for a reasonable initial brain segmentation. Details for the sensitivity of the filtering to the parameter values are given in [32]. The discrete diffusion process consists of updating each pixel in the image by an amount equal to the flow contributed by its four nearest neighbors. (Note that eight nearest neighbors can be used if the flow contribution of the diagonal neighbors is scaled according to their relative distance from the pixel of interest [20] and Anisotropic data can be handled similarly.)

We use 2-D nonlinear anisotropic diffusion to attenuate (darken) the skull and some other nonbrain regions in each MRI slice.[1] Using a simple low threshold, this allows the brain (and, inevitably, the eyes) to be segmented, as illustrated in Fig. 4. Without such filtering, a simple single-threshold-based segmentation would be difficult, if not impossible.

2) Automatic Threshold: Once each MRI slice has been diffused we segment the brain using a single automatically found threshold. We observed that the regularization of brain voxels achieved by diffusion filtering results in a brain voxel distribution that is close to normal for T2-weighted and even PD images. Thus the threshold level is determined by fitting a Gaussian curve to the histogram of the diffused volume. For PD and T2-weighted slices, the threshold is chosen at 2 standard deviations below the mean [8]. For T1-weighted axially displayed images, the threshold is chosen at the intensity at the minimum value in the brain histogram plot, which corresponds to about 0.5 standard deviations below the mean of the fitted Gaussian.[2] Fig. 5 shows the voxel-intensity histogram of a diffused T2-weighted volume with the best-fit Gaussian curve and threshold level overlaid. Fig. 6 shows a slice of the binary mask produced by the threshold.

3) Mask Refinement: The binary mask produced by automatic thresholding contains misclassified regions, such as the eyes [see Fig. 6(b)]. These regions are removed from each slice using morphology and spatial information provided by the head mask. First, holes are filled within each region of the mask. Next, binary erosion is performed to separate weakly connected regions. In all cases, the kernel used by the

[1] We also experimented with a 3-D nonlinear anisotropic diffusion filter over the entire MRI volume. 3-D diffusion, however, increased the partial volume effect, blurring the edges of the brain [32].

[2] The normal fit is not too good on diffused 3-D T1-weighted images and RF inhomogeneity may influence the choice of threshold on these thin slices, so we divide the 3-D volume data into sets of slices corresponding to about 8 cm, and segment each set separately with the appropriate threshold. The thresholds differ from each other by less than 2% of the maximum intensity in the whole volume.

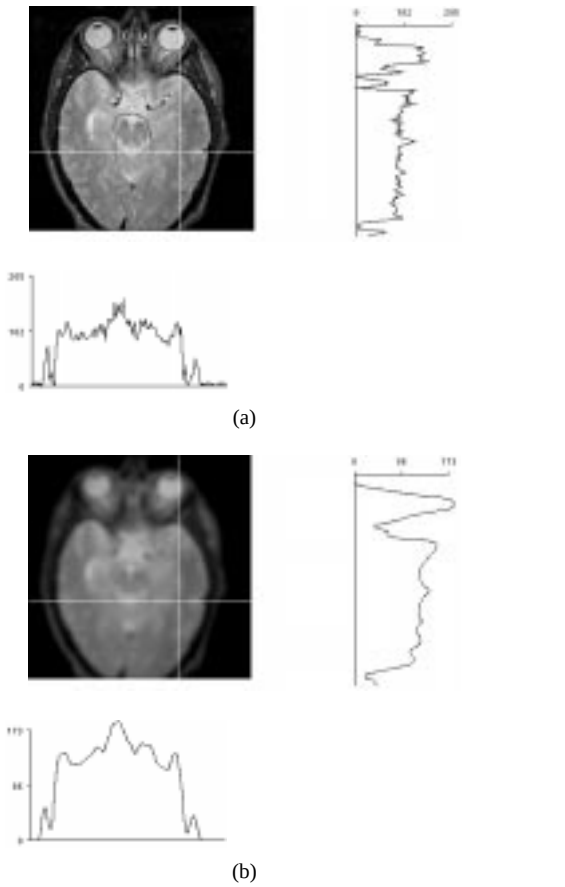

Fig. 4. Intracranial boundary detection using 2-D nonlinear anisotropic diffusion filtering. (a) Original T2-weighted image. (b) 2-D diffused image. Diffusion reduces nonbrain tissues, enabling a simple threshold to segment the brain.

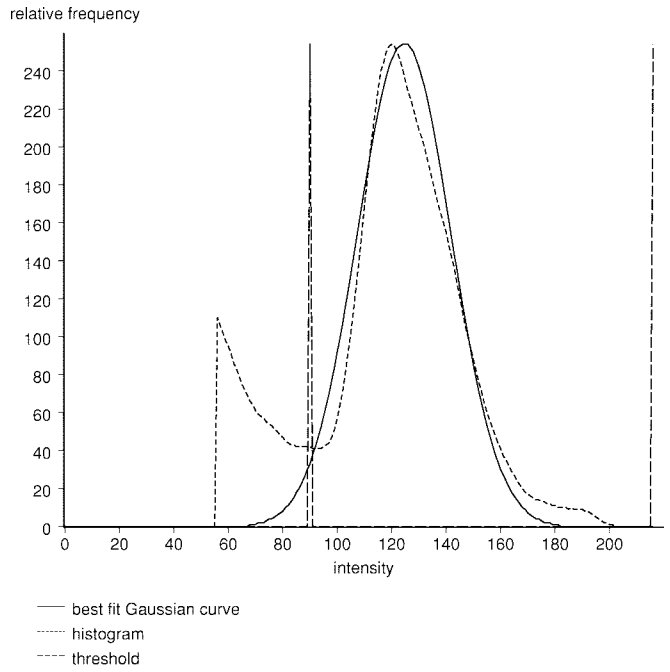

Fig. 5. A histogram of the diffused T2-weighted MR scan with the best-fit Gaussian curve and threshold levels overlaid.

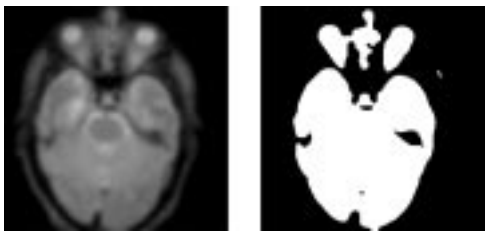

Fig. 6. A binary mask produced by automatic thresholding. (a) The diffused image slice. (b) The corresponding binary mask.

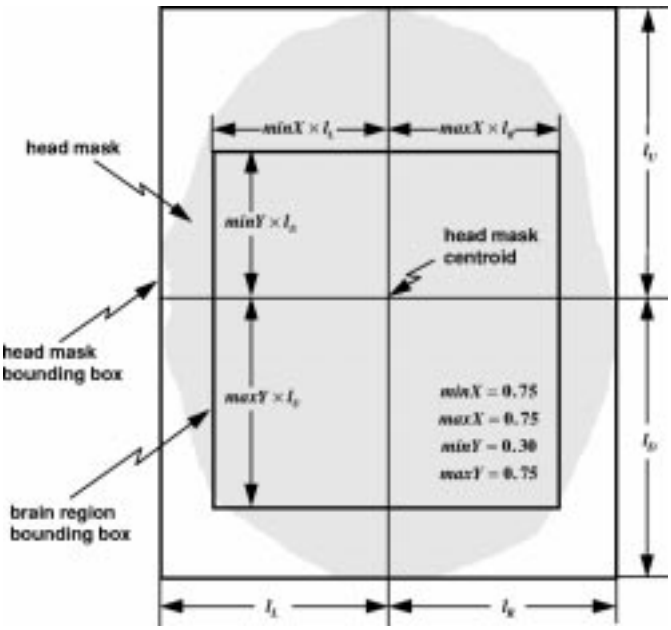

Fig. 7. Spatial information from the head mask is used to eliminate regions that are unlikely to correspond to brain tissue. Features whose centroids fall outside the *brain region bounding box* are discarded.

erosion is a 10×10 2-D binary matrix of ones except for the four corners which have six zeros symmetrically located. The resulting kernel is hexagonally symmetric, four-pixels wide at each edge. This kernel is wide enough to separate the eyes from the brain on the filtered thresholded volume in all axial slices we studied, with fields of view between 200 and 260 mm. After erosion, regions whose centroids fall outside a bounding box defined by the head mask are eliminated. This bounding box for axial slices with the eyes up is illustrated in Fig. 7. The given dimensions of the brain region bounding box were chosen experimentally to produce good results for all data sets with the eyes up, the same values being valid for several fields of view. A different set of parameters is required for images with the eyes down, and another for coronally and sagitally displayed images.[3] Finally, binary dilation, using the same 10×10 2-D kernel as for erosion, is performed on the remaining regions to return them close to their original size—this is necessary because the threshold already has eliminated the darkest pixels at the brain edge, and the final

[3] Sagitally displayed images require two bounding boxes because of the lack of symmetry in the images.

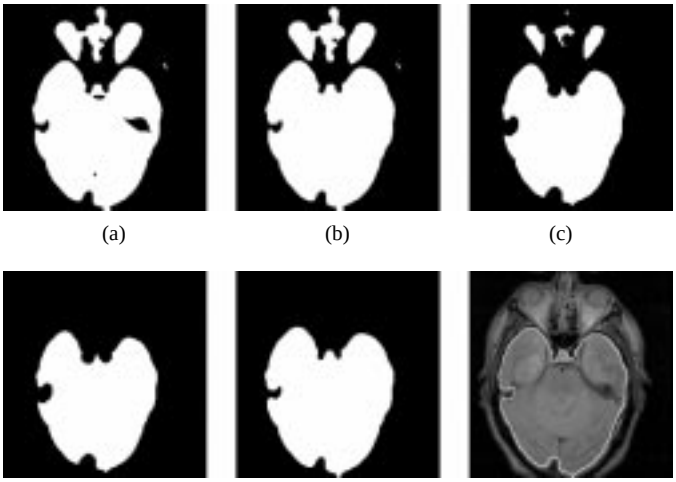

Fig. 8. Elimination of misclassified regions from the initial brain mask. The mask: (a) produced by thresholding, (b) after regions have been filled, (c) after binary erosion, (d) after elimination of nonbrain regions, and (e) after binary dilation. (f) Shows the initial brain mask overlaid on the PD-weighed slice.

step works best when the starting value is close to the required edge. The results of these steps are shown in Fig. 8.

D. Generate Final Brain Mask

Given the initial brain mask as a seed, we use an active contour model algorithm, extended from the "Snakes" algorithm introduced by Kass *et al.* [25], to locate the boundary between the brain and the intracranial cavity. The algorithm deforms the contours defined by the perimeter of the initial brain mask to lock onto the edge of the brain. Each active contour is defined as an ordered collection of n points in the image plane

$$V = \{v_1, \cdots, v_n\}$$
$$v_i = (x_i, y_i), \quad i = \{1, \cdots, n\}. \tag{6}$$

The points in the contour iteratively approach the intracranial boundary through the solution of an energy minimization problem. For each point v_i, an energy matrix $E(v_i)$ is computed

$$E(v_i) = \alpha E_{\text{cont}}(v_i) + \beta E_{\text{bal}}(v_i) + \gamma E_{\text{int}}(v_i) + \kappa E_{\text{grad}}(v_i) \tag{7}$$

where $E_{\text{cont}}(v_i)$ is a "*continuity*" energy function that influences the contour to take the shape of a circle, $E_{\text{bal}}(v_i)$ is an adaptive "*balloon*" force that pushes the contour outward until it reaches a strong gradient [10], $E_{\text{int}}(v_i)$ is an "*intensity*" energy function, computed from the PD-weighted MRI volume, that influences the contour to move toward low intensity regions, and $E_{\text{grad}}(v_i)$ is a "*gradient*" energy function, computed from the diffused MRI volume, that influences the contour to move toward regions of strong gradient. α, β, γ, and κ are scalar constants providing relative weightings of the energy terms. Each v_i is then iteratively moved to the point of minimum energy in its neighborhood, which corresponds to the smallest element in $E(v_i)$.

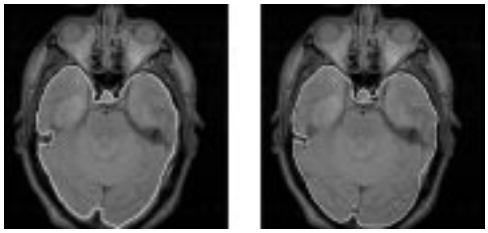

Fig. 9. Refinement of the intracranial contour. (a) The contour defined by the perimeter of the initial brain mask. (b) The intracranial contour detected using the active contour model algorithm.

The combination of energy functions described above enables the active contour model algorithm to detect the intracranial boundary in all image slices using the same relative energy weightings. The diffusion process ensures that the initial brain mask falls completely inside the brain. Therefore, the adaptive balloon force aides in cases where the initial brain mask is poor. The intensity energy term helps the active contour algorithm produce consistent results where partial volume effects are particularly severe. Finally, computing the gradient energy term from the diffused volume greatly stabilizes the active contour algorithm because the gradient derivatives are small in the diffused volume [32].

Fig. 9 illustrates the result of applying our active contour model algorithm to the MR slice shown in Fig. 8. It was found experimentally that a single setting of these parameters, $\alpha = 1$, $\beta = 2$, $\gamma = 1.5$, and $\kappa = 2$ produced good results on all data sets.[4]

III. Results

A. Brain Studies

Fig. 10 shows the intracranial contour detected automatically by our algorithm overlaid on selected slices of a PD-weighted MRI data set. The PD and T2 data sets were acquired axially on a GE 1.5 Tesla MRI scanner, with repetition time $\text{TR} = 2000$ ms, and echo times of 35 ms and 70 ms respectively. The data consists of 22 slices with 256×256 pixels per slice, scaled linearly from the original 12-bit data to 8 bits. The pixel size is 0.781 mm^2, and the slice thickness is 5 mm.

The intracranial boundary shown in Fig. 10 is accurate in all slices, except for the inclusion of the pituitary gland and basilar artery in slices 6 and 7, and insufficient exclusion of the petrous temporal bone in slice 5. However, the inclusion of pituitary gland and the petrous temporal bone is not a problem for subsequent analysis of the brain data.

Careful examination shows that the partial volume effect, particularly in the high slices, is dealt with in a consistent way.

Our algorithm produced comparable results for more than 30 other data sets from four other scanners with field-of-view varying from 200 to 260 mm, and also it worked on six images acquired on a GE scanner with a SPRG sequence, with $\text{TR} = 39$ ms and $\text{Te} = 8$ ms, pixel size $= 1.0156$ mm^2

[4] Details on the selection of these parameters are given in [32].

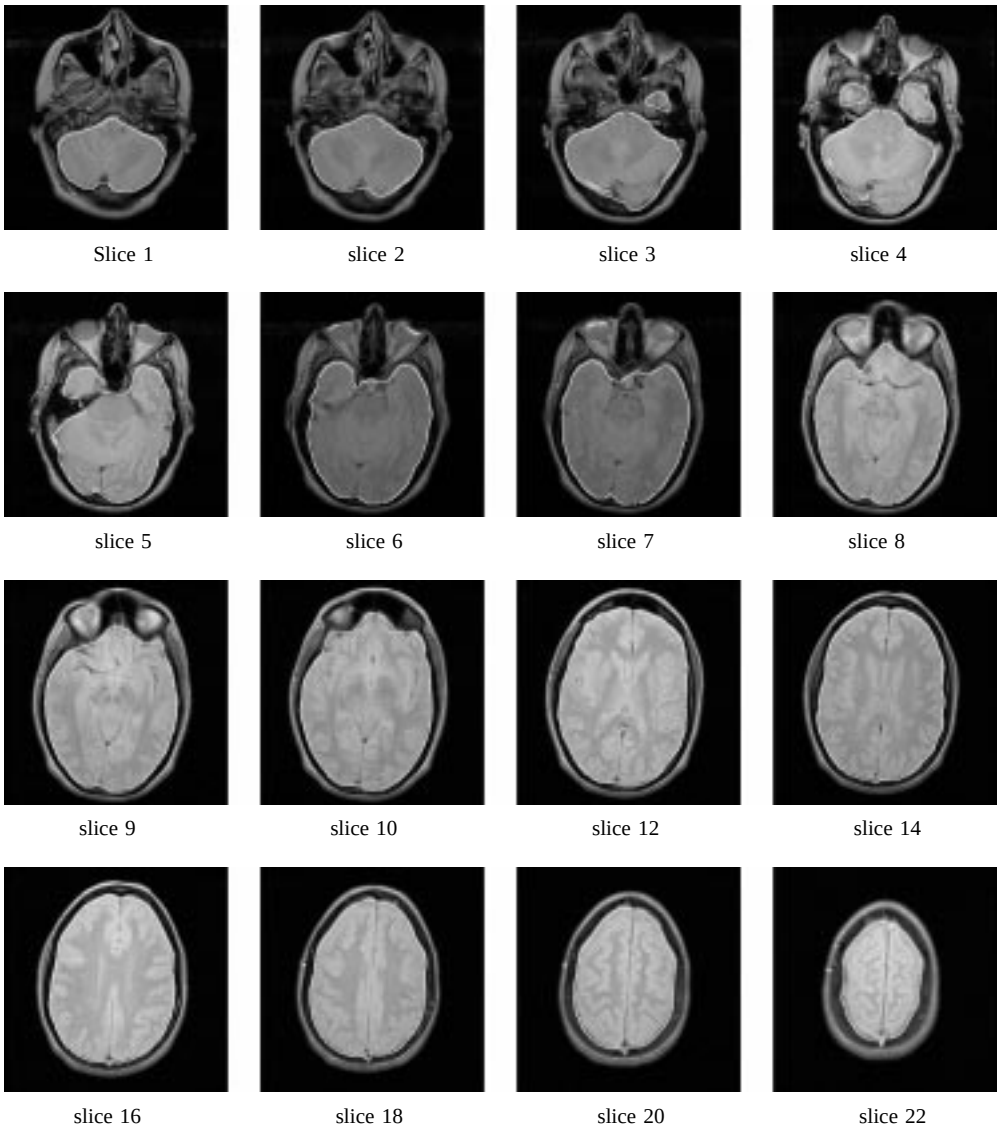

Fig. 10. An automatically detected intracranial contour overlaid on selected slices of a PD-weighed MRI scan.

and slice thickness = 2.5 mm. In all cases, our algorithm successfully detected the intracranial boundary without user interaction and without parameter modification.

B. Validation

The brain contours on seven complete scans were validated visually by a radiologist, and deemed to be sufficiently accurate for the purposes of MS lesion segmentation, and for multimodal image regsitration of photon emission tomography (PET)-MRI volumes.

Quantitative Validation Studies: Three volumes were chosen for quantitative validation by a radiologist; each volume was acquired using a different PD/T2-weighted echo sequence, and a different field of view size. For each volume, some axial slices were selected, such that the entire range of the image volume from "low" to "high" slices was covered. For each of these slices a radiologist traced the brain contour manually, and the manual brain contour was compared with the automatically drawn contour.

To quantify these results, we use the *similarity index* described by Zijdenbos [47], derived from a reliability measure known as the kappa statistic. Consider a binary segmentation as a set A containing the pixels considered to belong to the classification. The similarity of two segmentations A_1 and A_2 is given by a real number $S \in \{0 \cdots 1\}$ defined by

$$S = 2\frac{|A_1 \cap A_2|}{|A_1| + |A_2|}.$$

Because the similarity index is the ratio of twice the common area of the segmentations to the sum of the sizes of the individual areas, it is sensitive to both size and location. Therefore, two equally sized regions that overlap each other with half of their area results in $S = 1/2$ and a region completely overlapping a smaller one of half its size yields $S = 2/3$. This reflects the intuitive feeling that two regions, of which one fully encompasses the other, are more similar than two partially overlapping regions. Now Zijdenbos states that although $S > 0.7$ indicates excellent agreement, the absolute value of S is difficult to interpret; however, as an example,

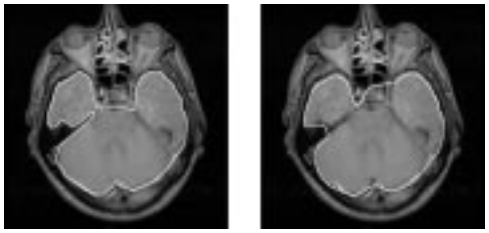

(a) (b)

Fig. 11. Comparison of manual contour with automatic contour. (a) The intracranial contour manually drawn by a radiologist. (b) The intracranial contour detected using the active contour model algorithm. The similarity index of these two contours is 0.942.

TABLE I
COMPARISON OF MANUAL AND AUTOMATIC BRAIN SEGMENTATION

Dataset	Slice number	Manual area (pixels)	Auto area (pixels)	Similarity index
1	4	8912	10269	0.925
1	7	20264	22472	0.929
1	8	22035	23918	0.954
1	23	20109	20341	0.980
1	24	15909	17201	0.958
1	25	12122	13194	0.952
2	2	15386	16549	0.942
2	6	25935	26072	0.986
2	12	27402	27346	0.9
3	7	14705	15639	0.961
3	8	17648	18645	0.967
3	17	17552	18027	0.984

the similarity index of the two images in Fig. 11(a) and (b) is 0.942.

Results are given in Table I, which shows the number of pixels included inside the manually drawn and automatically calculated brain contours, together with the similarity index.

In axial slices containing the eyes, the automatic method usually included the pituitary gland and basilar artery, and sometimes the internal carotid artery, whereas the radiologist excluded these (see Fig. 10 slice 6 and 7). Also, the petrous temporal bone was often included in the automatic method [see Fig. 9(b)], whereas the radiologist drew carefully around it. One of these eye slices (Dataset 2, slice 2) is shown in Fig. 11, where the radiologist's manually drawn contour is shown in Fig. 11(a) and the automatically defined contour is shown in Fig. 11(b).

In the high slices, the manually drawn outlines were comparable to the automatically drawn outlines except in the extreme case of the top slice of the 5-mm-thick datasets where the partial volume effect was noticeable. Also, the sagittal sinus was always excluded by the radiologist, whereas the automatic routine usually included it (see Fig. 10 slices 18, 20, and 22).

The similarity between the automatic brain contour and the manual brain contour was very high—always above 0.925, best at 0.99 on middle slices, and dropping to 0.95 on the highest slices. These results compare very favorably with those reported by other researchers [1], [24] as the brain volumes are within 4% in most cases.

To measure the intra-observer accuracy, the radiologist performed two independent tracings of the brain contours. The enclosed brain pixels were within 96%–97% of each other with a similarity of around 0.98 between tracings. Hence the method is not expected to be more than 96% accurate as a measure of brain volume; however, the brain edge discrepencies do not have a significant impact on subsequent processing (e.g., MS lesions do not occur in the pituitary gland, and bone can be removed by simple thresholding).

IV. CONCLUSION

We have introduced a novel, fully automatic intracranial boundary detection algorithm that has proven effective on clinical and research MRI data sets acquired from several different scanners. The algorithm consists of three incremental steps. The first step uses histogram analysis to localize the head, providing a region which must completely surround the brain. The second step uses nonlinear anisotropic diffusion and automatic thresholding to create a mask that isolates the brain within the detected head region. Using this mask as a seed, the final step employs an active contour model algorithm to detect the intracranial boundary. This algorithm has proven robust in the presence of RF inhomogeneity and partial volume effects.

Our MRI brain segmentation algorithm is in regular use for studies of Multiple Sclerosis lesions, for studies of MRI-PET registration, and for studies involving image compression, where the nonbrain region is automatically given a higher compression ratio than the brain region in the images.

A. Future Work

We plan to work with the research 3-D sagittal MP-RAGE volumes, to determine good diffusion filter parameters so that a single threshold can be found for the brain, as our algorithm currently fails to include all the cortical regions of the brain for these images.

We also plan to extend the principles generated for automatic brain segmentation to the problem of lung segmentation for use in studies of lung diseases such as cystic fibrosis and emphysema, where the volume of the lungs is needed. A reliable consistent method for outlining the lungs is required for MR chest images. Early results with MR images are promising, and will be continued.

ACKNOWLEDGMENT

The authors would like to thank Dr. B. Wong of the University of British Columbia Hospital for providing expert advice and for manually outlining the brain contours. They would also like to thank Dr. D. Paty and Dr. D. Li of the University of British Columbia MS/MRI Group for providing some of the MRI data on which the algorithms were tested. They would also like to thank Dr. A. MacKay, Dr. K. Whittall, A. Riddehough, and K. Cover of the University of British Columbia MS/MRI Group for providing expert advice and Dr. C. DeCarli from the NIH, for providing some of MRI data sets used in these studies. Finally, they would like to thank the anonymous referees for their constructive criticism of the earlier drafts of this manuscript.

REFERENCES

[1] G. B. Aboutanos and B. M. Dawant, "Automatic brain segmentation and validation: Image-based versus atlas-based deformable models," in *Proc. SPIE-Medical Imaging 1997*, Feb. 1997, vol. 3034, pp. 299–310.

[2] L. Alvarez, P.-L. Lions, and J.-M. Morel, "Image selective smoothing and edge detection by nonlinear diffusion," *SIAM J. Number Anal.*, vol. 29, no. 3, pp. 845–866, June 1992.

[3] T. Arden and J. Poon, *WiT User's Guide*. Logical Vision Ltd., Burnaby, Canada, Oct. 1993, Version 4.1.

[4] M. S. Atkins and B. Mackiewich, "Automatic segmentation of the brain in MRI," in *Proc. Visualization in Biomedical Computing'96*,Sept. 1996, vol. 1131, pp. 210–216.

[5] M. S. Atkins, T. Zuk, B. Johnston, and T. Arden, "Role of visual languages in developing image analysis algorithms," in *Proc. IEEE Conf. Visual Languages*, St. Louis, MO, Oct. 1994, pp. 262–269.

[6] C. I. Attwood, G. D. Sullivan, and K. D. Baker, "Recognizing cortical sulci and gyri in MR images," in *Proc. British Machine Vision Conf.*, P. Mowforth, Ed., 1991.

[7] J. C. Bezdek, L. O. Hall, and L. P. Clarke, "Review of MR image segmentation techniques using pattern recognition," *Med. Phys.*, vol. 20, no. 4, pp. 1033–1048, 1993.

[8] M. E. Brummer, R. M. Mersereau, R. L. Eisner, and R. R. J. Lewine, "Automatic detection of brain contours in MRI data sets," *IEEE Trans. Med. Imag.*, vol. 12, pp. 153–166, June 1993.

[9] A. Chakraborty, L. H. Staib, and J. S. Duncan, "An integrated approach to boundary finding in medical images," in *Proc. IEEE Workshop on Biomedical Image Analysis*, Los Alamos, CA, June 1994, pp. 13–22.

[10] V. Chalana, W. Costa, and Y. Kim, "Integrating region growing and edge detection using regularization," in *Proc. SPIE Conf. Medical Imaging*, 1995.

[11] L. P. Clarke, R. P. Velthuizen, M. A. Camacho, J. J. Heine, M. Vaidyanathan, L. O. Hall, R. W. Thatcher, and M. L. Silbiger, "MRI segmentation: Methods and applications," *Magn. Reson. Imag.*, vol. 13, no. 3, pp. 343–368, 1995.

[12] H. E. Cline, W. E. Lorensen, R. Kikinis, and F. Jolesz, "Three-dimensional segmentation of MR images of the head using probability and connectivity," *J. Comput. Assist. Tomogr.*, vol. 14, no. 6, pp. 1037–1045, Nov./Dec. 1990.

[13] D. L. Collins, G. Le Goualher, R. Venugopal, A. Caramanos, A. C. Evans, and C. Barillot, "Cortical constraints for nonlinear cortical registration," in *Proc. Visualization in Biomedical Computing'96*, Sept. 1996, vol. 1131, pp. 307–316.

[14] C. A. Davatzikos and J. L. Prince, "An active contour model for mapping the cortex," *IEEE Trans. Med. Imag.*, vol. 14, pp. 65–80, Mar. 1995.

[15] D. Dean, P. Buckley, F. Bookstein, J. Kamath, D. Kwon, L. Friedman, and C. Lys, "Three dimensional MR-based morphometric comparison of schizophrenic and normal cerebral ventricles," in *Proc. Visualization in Biomedical Computing'96*, Sept. 1996, vol. 1131, pp. 363–372.

[16] P. Van den Elsen, J. B. A. Maintz, E.-J. D. Pol, and M. Viergever, "Automatic registration of CT and MR brain images using correlation of geometrical features," *IEEE Trans. Med. Imag.*, vol. 14, pp. 384–395, June 1995.

[17] W. A. Edelstein, P. A. Bottomley, and L. M. Pfeifer, "A signal-to-noise calibration procedure for NMR imaging systems," *Med. Phys.*, vol. 11, no. 2, pp. 180–185, 1984.

[18] P. A. Freeborough and N. C. Fox, "Assessing patterns and rates of brain atrophy by serial MRI: A segmentation, registration, display and quantification procedure," in *Proc. Visualization in Biomedical Computing'96*, Sept. 1996, vol. 1131, pp. 419–428.

[19] Y. Ge, J. M. Fitzpatrick, B. Dawant, J. Bao, R. Kessler, and R. Margolin, "Accurate localization of cortical convolutions in MR brain images," *IEEE Trans. Med. Imag.*, vol. 15, pp. 418–428, Aug. 1996.

[20] G. Gerig, O. Kübler, R. Kikinis, and F. A. Jolesz, "Nonlinear anisotropic filtering of MRI data," *IEEE Trans. Med. Imag.*, vol. 11, no. 2, pp. 221–232, June 1992.

[21] M. Henkelman, "Measurement of signal intensities in the presence of noise in MR images," *Med. Phys.*, vol. 12, no. 2, pp. 232–233, 1985.

[22] B. Johnston, M. S. Atkins, and K. S. Booth, "Partial volume segmentation in 3-D of lesions and tissues in magnetic resonance images," in *Proc. SPIE-Medical Imaging 1994*, Bellingham, WA, 1994, vol. 2167, pp. 28–39,

[23] B. Johnston, M. S. Atkins, B. Mackiewich, and M. Anderson, "Segmentation of multiple sclerosis lesions in intensity corrected multispectral MRI," *IEEE Trans. Med. Imag.*, vol. 15. pp. 154–169, Apr. 1996.

[24] T. Kapur, W. E. L. Grimson, W. M. Wells III, and R. Kikinis, "Segmentation of brain tissue from magnetic resonance images," *Med. Imag. Anal.*, vol. 1, no. 2, 1996.

[25] M. Kass, A. Witkin, and D. Terzopoulos, "Snakes: Active contour models," *Inte. J. Comput. Vision*, pp. 321–331, 1988.

[26] F. Lachmann and C. Barillot, "Brain tissue classification from MRI data by means of texture analysis," in *Proc. SPIE: Medical Imaging VI: Image Processing*, Chapel Hill, N.C., 1992, vol. 1652, pp. 72–83.

[27] C. Li, D. B. Godlgof, and L. O. Hall, "Knowledge-based classification and tissue labeling of MR images of human brain," *IEEE Trans. Med. Imag.*, vol. 12, pp. 740–750, Dec. 1993.

[28] H. Li, R. Deklerk, B. De Cuyper, A. Hermanus, E. Nyssen, and J. Cornelis, "Object recognition in brain CT-scans: Knowledge-based fusion of data from multiple feature extractors," *IEEE Trans. Med. Imag.*, vol. 14, pp. 212–229, June 1995.

[29] K. O. Lim and A. Pfefferbaum, "Segmentation of MR brain images into cerebrospinal fluid spaces, white and gray matter," *J. Comput. Assist. Tomogr.*, vol. 13, no. 4, pp. 588–593, July/Aug. 1989.

[30] S. Lobregt and M. Viergever, "A discrete dynamic contour model," *IEEE Trans. Med. Imag.*, vol. 14, pp. 12–24, Mar. 1995.

[31] A. Lundervold and G. Storvik, "Segmentation of brain parenchyma and cerebrospinal fluid in multipspectral magnetic resonance images," *IEEE Trans. Med. Imag.*, vol. 14, pp. 339–349, June 1995.

[32] B. Mackiewich, "Intracranial boundary detection and radio frequency correction in magnetic resonance images," M.S. thesis, Simon Fraser Univ., Burnaby, B.C., Canada, Aug. 1995.

[33] N. Nordström, "Biased anisotropic diffusion—A unified generalization and diffision aapproach to edge detection," *Image Vision Comput.*, vol. 8, no. 4, pp. 318–327, 1990.

[34] F. Pannizzo, M. J. B. Stallmeyer, J. Friedman, R. J. Jennis, J. Zabriskie, C. Pland, R. Zimmerman, J. P. Whalen, and P. T. Cahill, "Quantitative MRI studies for assessment of multiple sclerosis," *Magn. Reson. Med.*, vol. 24, pp. 90–99, 1992.

[35] D. W. Paty, "Interferon beta-1b in the treatment of multiple sclerosis: Final outcome of the randomized controlled trial," *Neurol.*, vol. 45, pp. 1277–1285, July 1995.

[36] D. W. Paty and D. K. B. Li, "Interferon beta-1b is effective in relapsing-remitting multiple sclerosis. ii. MRI analysis results of a multicenter, randomized, double-blind, placebo-controlled trial," *Neurol.*, vol. 43, pp. 662–667, Apr. 1993.

[37] P. Perona and J. Malik, "Scale-space and edge detection using anisotropic diffusion," *IEEE Trans. Pattern Anal. Machine Intell.*, vol. 12, pp. 629–639, July 1990.

[38] S. Ranganath, "Contour extraction from cardiac MRI studies using snakes," *IEEE Trans. Med. Imag.*, vol. 14, pp. 328–338, June 1995.

[39] G. Sapiro and A. Tannenbaum, "Edge preserving geometric smoothing of MRI data," Univ. Minnisota, Dept. of Electrical Engineering, Tech. Rep., Apr. 1994.

[40] J. W. Snell, M. B. Merickel, J. M. Ortega, J. C. Goble, J. R. Brookeman, and N. F. Kassell, "Segmentation of the brain from 3-D MRI using a hierarchical active surface template," in *Proc. SPIE Conf. Medical Imaging*, 1994.

[41] L. H. Staib and J. S. Duncan, "Boundary finding with parametrically deformale models," *IEEE Trans, Pattern Anal. Machine Intell.*, Nov. 1992.

[42] R. R. Stringham, W. A. Barrett, and D. C. Taylor, "Probabilistic segmentation using edge detection and region growing," in *Proc. SPIE: Visualization in Biomedical Computing 1992*, Chapel Hill, N.C., 1992, vol. 1808, pp. 40–51.

[43] H. Suzuki and J. Toriwaki, "Automatic segmentation of head MRI images by knowledge guided thresholding," *Computerized Med. Imag., Graphics*, vol. 15, no. 4, pp. 233–240, July–Aug. 1991.

[44] D. R. Thedens, D. J. Skorton, and S. R. Fleagle, "Methods of graph searching for border detection in image sequences with applications to cardiac MRI," *IEEE Trans. Med. Imag.*, vol. 14, pp. 42–55, Mar. 1995.

[45] K. L. Vincken, A. S. E. Koster, and M. A. Viergever, "Probabilistic multiscale image segmentation—set-up and first results," in *Proc. SPIE: Medical Imaging VI: Image Processing*, Chapel Hill, N.C., 1992, vol. 1808, pp. 63–77.

[46] W. M. Wells, III, W. E. L. Grimson, R. Kikinis, and F. A. Jolesz, "Adaptive segmentation of MRI data," *IEEE Trans. Med. Imag.*, vol. 15, pp. 429–443, Aug. 1996.

[47] A. P. Zijdenbos, B. M. Dawant, R. A. Margolin, and A. C. Palmer, "Morphometric analysis of white matter lesions in MR images: Method and validation," *IEEE Trans. Med. Imag.*, vol. 13, p. 4, pp. 716–724, Dec. 1994.